



OPEN ACCESS

EDITED BY

Michele Celebrano,
Polytechnic University of Milan, Italy

REVIEWED BY

Andrea Tognazzi,
University of Palermo, Italy
Shengxuan Xia,
Hunan University, China

*CORRESPONDENCE

Nasim Mohammadi Estakhri,
✉ estakhri@chapman.edu

RECEIVED 24 March 2023

ACCEPTED 01 June 2023

PUBLISHED 30 June 2023

CITATION

Didari-Bader A, Estakhri NM and
Mohammadi Estakhri N (2023), Adaptive
plasmonic metasurfaces for radiative
cooling and passive thermoregulation.
Front. Photonics 4:1193479.
doi: 10.3389/fphot.2023.1193479

COPYRIGHT

© 2023 Didari-Bader, Estakhri and
Mohammadi Estakhri. This is an open-
access article distributed under the terms
of the [Creative Commons Attribution
License \(CC BY\)](https://creativecommons.org/licenses/by/4.0/). The use, distribution or
reproduction in other forums is
permitted, provided the original author(s)
and the copyright owner(s) are credited
and that the original publication in this
journal is cited, in accordance with
accepted academic practice. No use,
distribution or reproduction is permitted
which does not comply with these terms.

Adaptive plasmonic metasurfaces for radiative cooling and passive thermoregulation

Azadeh Didari-Bader¹, Nooshin M. Estakhri² and
Nasim Mohammadi Estakhri^{1*}

¹Fowler School of Engineering, Chapman University, Orange, CA, United States, ²Department of Physics, Virginia Tech, Blacksburg, VA, United States

In this work, we investigate a class of planar photonic structures operating as passive thermoregulators. The radiative cooling process is adjusted through the incorporation of a phase change material (Vanadium Dioxide, VO₂) in conjunction with a layer of transparent conductive oxide (Aluminum-doped Zinc Oxide, AZO). VO₂ is known to undergo a phase transition from the “dielectric” phase to the “plasmonic” or “metallic” phase at a critical temperature close to 68°C. In addition, AZO shows plasmonic properties at the long-wave infrared spectrum, which, combined with VO₂, provides a rich platform to achieve low reflections across the atmospheric transparency window, as demanded in radiative cooling applications, while also maintaining a compact size. Using numerical analysis, we study two classes of patterned and non-patterned compact multilayer metal-dielectric-metal metasurfaces, aiming to maximize the overall absorption in the first atmospheric transparency window (8–13 μm) while maintaining a high reflection across the solar spectrum (0.3–2.5 μm). Surfaces are initially designed based on a round of coarse optimization and further improved through analyzing the impact of geometric parameters such as size and periodicity of the metasurface elements. Our findings are relevant to applications in thermal regulation systems and passive radiative cooling of high-temperature devices, such as electronic elements.

KEYWORDS

radiative cooling, thermoregulation, transparent conducting oxides (TCOs), phase-change materials (PCM), metasurfaces, adaptive photonics

1 Introduction

Energy consumption and the global demand for cooling are predicted to increase tenfold by 2050 (Goldstein, Raman and Fan, 2017). This sudden surge, both in residential and commercial areas, brings in the need for alternative solutions to compensate for the rise in energy consumption. Specifically, over the past decade, the need for alternate daytime and night-time cooling solutions for buildings, solar cells, and electronic devices has created an increased interest in passive radiative cooling approaches (Raman et al., 2014; Sun et al., 2017; Wang et al., 2021). Designer nanophotonic systems have been employed to realize radiative cooling (Assaworrorarit, Omair and Fan, 2022; Choi et al., 2022; Fan and Li, 2022; Li et al., 2022; Didari-Bader and Menguc, 2023) through selective design approaches that involve a combination of carefully selected materials and engineered structural parameters.

Metamaterials, metasurfaces, and multilayered thin-film structures (Kecebas et al., 2017; Didari and Mengüç, 2018; Bijarniya, Sarkar and Maiti, 2020; Perrakis et al., 2020; Kim et al., 2021; Yin et al., 2021; Araki and Zhang, 2022; Chamoli et al., 2022; Jin, Jeong and Yu, 2022; Lee et al., 2022; Cai et al., 2018; Gentle et al., 2018; Sun et al., 2018a; Zhao et al., 2020; Qin et al., 2022; Sun et al., 2022a; Sun et al., 2022b) have been explored for realizing temperature-adaptive devices for radiative cooling purposes. Meta-structures have been proven to outperform conventional structures for radiative cooling applications, as they provide more degrees of freedom to strategically optimize the performance of the system (Lee et al., 2022). Ideal daytime radiative coolers need to achieve relatively high reflection within the solar spectrum and simultaneously high emission (absorption) within the atmospheric transparency windows. Depending on the desired application, various considerations should be made when designing a radiative cooler, including the ambient and targeted temperatures, broadband or narrowband spectral emissivity, and the choice of material.

Passive temperature-switchable cooling is an especially appealing progression of the more traditional passive radiative cooling approaches, allowing for temperature-regulated responses. The self-regulatory temperature can be achieved through the incorporation of phase-change materials, which then creates a temperature-sensitive response due to the phase-change transition from metallic to dielectric states and *vice versa*. Metasurface configurations have shown to be successful candidates for these devices as they can provide enhanced and controllable wave matter interaction over subwavelength-scale volumes. Recently, smart thermal emitters based on VO₂ on Silicon dioxide (SiO₂) spacers have been proposed to achieve enhanced infrared absorption (Sun et al., 2018b) along with high visual transparency (Sun et al., 2022b) for radiative cooling in terrestrial and space applications. In addition, multilayer VO₂-based coatings (Ono et al., 2018; Araki and Zhang, 2022), scalable micro-structured VO₂ metasurfaces (Long, Taylor and Wang, 2020), as well as the incorporation of other phase change materials such as In₃SbTe₂, have been recently studied for switchable infrared emission and/or radiative cooling (Zha et al., 2022). In this work and building upon the previous advances in switchable radiative cooling metasurfaces, we study two self-adaptive layered metasurfaces with patterned and non-patterned VO₂ top layers. Different dielectric spacers and a secondary plasmonic layer (AZO) are incorporated into the design to take advantage of possible coupling to guided modes (Abass et al., 2012) to enhance emissivity within the atmospheric window. The non-patterned structures are first optimized for the thickness of each layer for both high reflectivity and high emissivity within the solar spectrum and atmospheric transparency window, respectively. Patterning the phase-change material is also used to improve the spectral responses. Our findings also show that when VO₂ has a dielectric response (cold state), geometric manipulation has no significant effect on the tunability of the optical response of these structures. We will expand on these discussions in section 2, where we discuss material selection, design, and methodologies, followed by results and discussions in section 3.

2 Material selection, design, and methodology

2.1 Material selection

In this work, we analyze the optical response of two self-adaptive planar metasurfaces for their potential use in passive radiative cooling applications. The proposed structures are composed of phase-change materials (PCMs) (Ono et al., 2018; Zhang et al., 2018; Sato and Yamada, 2019; Ko, Badloe and Rho, 2021), transparent conducting oxides (TCOs) (Lewis and Paine, 2000; Abb et al., 2014; Sun et al., 2018a), and plasmonic (Xia et al., 2017; 2022) and dielectric materials. Each of these material categories plays a unique role in tailoring the reflection and absorption properties of the structures under study within the visible and infrared spectrums. In this section, we briefly review material characteristics for PCMs and TCOs and their functionalities in radiative cooling applications.

2.1.1 Phase-change material selection

PCMs enable a plethora of applications in tunable nanophotonic structures including tuning the response of infrared antennas and metasurfaces, optical limiting and optical diodes, and tuning quantum two-photon interference, to name a few (Morin, 1959; Wang et al., 2016; Butakov et al., 2018; Wan et al., 2018; Howes et al., 2020; Estakhri and Norris, 2021; Irfan Lone and Jilte, 2021; Wan et al., 2021; Song et al., 2022; Li et al., 2023; Tognazzi et al., 2023). In radiative cooling processes, PCMs such as VO₂ that undergo a metal-to-insulator transition at certain temperatures can potentially act as a switch that has “off” and “on” states (Cui et al., 2018; Ono et al., 2018). In high-temperature conditions and when addressing excessive heat, such a PCM-based structure is switched on to facilitate the cooling process. This results in high emissivity within the atmospheric transparency window. When the environment under the study has cooled down, the PCMs that undergo metal-to-insulator transition act in the “off” state, allowing reduced emissivity throughout the infrared spectrum. Therefore, preventing further cooling down. Here, we use a well-studied PCM, VO₂, as thermal switch. Pristine VO₂ exhibits a transition from insulator to metallic state at a critical temperature of 68°C (Sun et al., 2022b). We note that the exact transition temperature of VO₂ depends on the film thickness and the substrate material (Wan et al., 2019), thus might be slightly different from the nominal value for different designs. VO₂ can be fabricated using atomic layer deposition, which provides great control over the thickness and uniformity of the layers (Currie, Mastro and Wheeler, 2018). It is also possible to reduce the critical temperature at which VO₂ experiences its phase change through co-doping of other materials, such as Tungsten and Strontium, into pristine VO₂ (Ono et al., 2018). These key properties exhibit VO₂ as a fitting choice for radiative cooling applications.

2.1.2 Transparent conducting oxide selection

TCOs (Lewis and Paine, 2000) are a class of materials that are electrically conductive, yet they can be optically transparent. In addition, and based on their free-electron density (i.e., by adding electron donor dopants), these materials can be tuned to achieve a dielectric phase in the visible and a metallic response in the near-

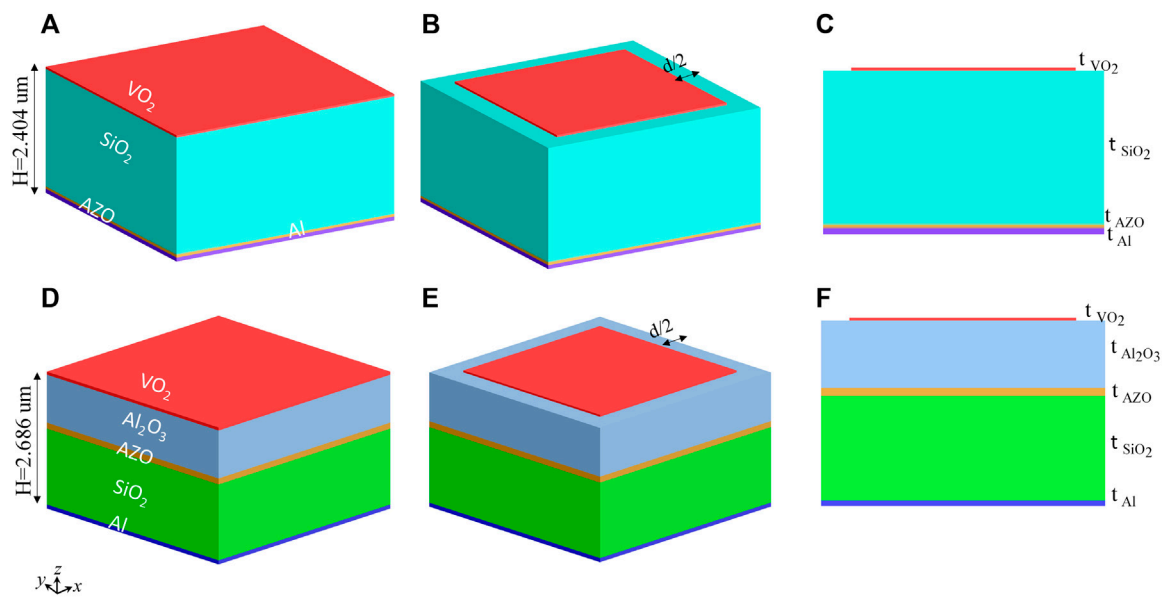


FIGURE 1

3D rendering of the (A, D) non-patterned and (B, E) unit cell of the patterned metasurfaces studied in this work. The four-layer system consists of a SiO_2 layer sandwiched between thin layers of VO_2 and AZO, placed on an Al substrate (A–C). The metal-backed five-layer system consists of VO_2 , Al_2O_3 , AZO, SiO_2 , and Al (D–F). (C, F) Cross-sections of the patterned structures (with x and y periodicity of “L”) where the top VO_2 layer is replaced with square VO_2 patches. The optimized values for all thicknesses are provided in the main text.

and far-infrared spectrum range (Sun et al., 2018a). TCOs can be fabricated with various techniques such as sputtering, evaporation, atomic layer deposition, and pulsed laser deposition, allowing for accurate thickness control and nano-scale-thin layer fabrication (Sun et al., 2018a). Here, we incorporated a layer of AZO in our proposed designs which creates a transition from dielectric characteristics in the visible and near-infrared range into a metallic phase in the mid-infrared range.

2.2 Design

Schematics of the proposed layered structures are shown in Figure 1. We consider the case of a four-layer surface, as illustrated in Figures 1A–C and a five-layer surface, as illustrated in Figures 1D–F. Both structures are placed on a reflective Aluminum (Al) ground, and the VO_2 and AZO layers are separated with a dielectric spacer in each case (Sun et al., 2022b). The first spacer (SiO_2) shows an absorption peak around $10\ \mu\text{m}$ which is within the first atmospheric transparency window, while the second spacer (Aluminum Oxide, Al_2O_3) is low loss across this range, with an absorption peak in longer wavelengths (E.D. Palik ed., 1998). Both spacers are low-index and lossless across the visible spectrum. To take advantage of the high absorption in SiO_2 while masking the sharp transitions occurring around $10\ \mu\text{m}$, the layer of SiO_2 is placed below the AZO layer in the five-layer configuration. Relevant geometric parameters are provided in the figure. Parameters “L” and “d” are only relevant to the patterned surface, while all the other parameters are kept constant between patterned and non-patterned scenarios.

In the first step, genetic algorithm is used to optimize the thickness of the layers in both structures, aiming at simultaneously maximizing absorption within the atmospheric transparency window and maximizing reflection within the solar spectrum range. More details on the optimization are provided in Section 2.3. As a result of this optimization, for the four-layer structure, we chose Al, AZO, SiO_2 , and VO_2 thicknesses to be 165 nm, 25 nm, 2,200 nm, and 14 nm, respectively. Similarly, for the five-layer structure, we set the thicknesses of Al, AZO, SiO_2 , Al_2O_3 , and VO_2 layers at 80, 1,500, 120, 970, and 16 nm, respectively. Accordingly, the total height of the four-layer structure is $H = 2.404\ \mu\text{m}$, and the height of the five-layer structure is $H = 2.686\ \mu\text{m}$, well within the range of conventional metasurfaces.

2.3 Methodology

2.3.1 Genetic optimization algorithm

The first stage of the design is a coarse optimization to set the thickness of each layer. See the end of the Design section for the parameter values. At this stage, we exclude the effect of the VO_2 patterning, i.e., the optimization is performed only for the layered non-patterned surfaces. This allows us to significantly reduce the computational cost of the optimization while creating a good baseline for the design of the patterned structures. Indeed, and as it will be discussed later, we observed that the main effect of VO_2 patterning is through localized resonances at the corners. Consequently, this initial optimization operates in conjunction with the patterning effect to boost the performance of the device.

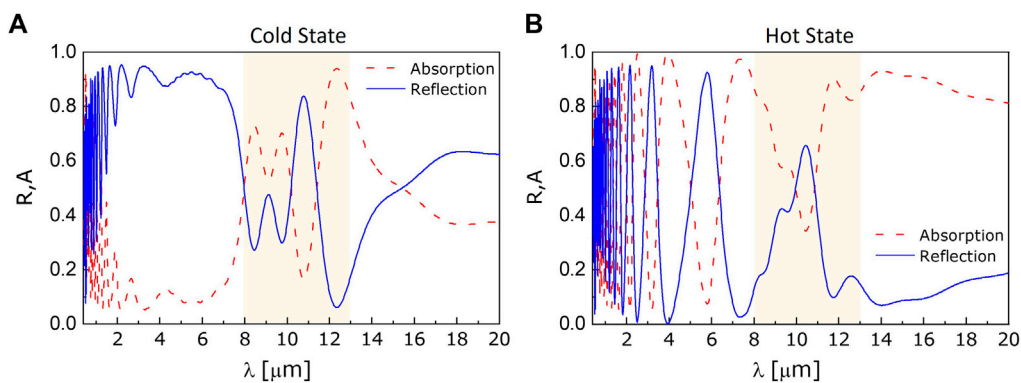


FIGURE 2

Absorption (red-dashed) and reflection (blue-solid) spectra for the four-layer structure shown in Fig.1(A) at (A) cold and (B) hot states.

MATLAB embedded genetic algorithm optimization is used (Matlab, 2023) to maximize reflection and absorption across 0.2–2.5 μm and 8–20 μm , respectively. Specifically, reflection is calculated at 50 nm intervals across 0.2–2.5 μm (47 points), and absorption is calculated at 0.5 μm intervals across 8–20 μm (25 points). Optimization goal is set to minimize $\left(\sum_{\lambda_1}^{\lambda_{25}} \text{Absorption}\right)^{-1} + 0.5\left(\sum_{\lambda_1}^{\lambda_{47}} \text{Reflection}\right)^{-1}$, resulting in two simultaneous goals focusing on enhancing the absorption in the second band while still maintaining high reflections in the first band. Due to the highly oscillatory behavior of the response across shorter wavelengths which are mainly associated with Fabry-Perot resonances in thick dielectric spacers (e.g., see Figure 2), more data points are used over this range.

2.3.2 Finite difference time domain method

After the thickness values are set through the initial optimization process, we conduct a 3D finite difference time domain (FDTD) analysis to obtain the reflection, absorption, and transmission spectra of both structures (Lumerical, 2023). In this study, the excitation source is a plane wave illuminating perpendicularly from the top of the structure along the negative z -axis (see Figure 1). In terms of boundary conditions in the numerical studies, we adopted periodic boundary conditions in the x and y directions and a perfectly matched layer (PML) along the z -axis. Two 2D z -normal monitors are placed to record the reflection and transmission spectra of fields. To deal with very thin films, advanced mesh refinement is used, and an extra mesh layer is applied to increase the accuracy of the calculated fields across the structures and at the intersection between layers. The wavelength range of interest in our simulations is 0.4–20 μm .

2.3.3 Finite element simulations and mode analysis

The field profiles presented in the next section and the modal analysis reported in the text are performed in the COMSOL RF solver (COMSOL, 2023). For the simulation of the patterned metasurface, the minimum/maximum mesh sizes are set to 20/100 nm for the AZO and Al layers, 50/200 nm for dielectric layers, 3/

50 nm for the VO₂ patch, and 80/300 nm for the air region. For mode analysis simulations in non-patterned structures, the minimum mesh size is set to 2 nm throughout the whole structure. The maximum mesh size is set to 5 nm in Al, VO₂ and AZO layers and 200 nm in SiO₂, Al₂O₃, and air regions.

3 Results and discussions

3.1 Four-layer structure

The FDTD results for the reflection and absorption spectra of the four-layer metasurface at both the cold state and hot state (referring to temperatures lower and higher than the critical temperature of the pristine VO₂) are depicted in Figure 2. When VO₂ is in the hot state (Figure 2B), a relatively high reflection within the solar spectrum is observed. Inspecting the atmospheric transparency window, absorption is significantly higher than the cold state; however, it experiences a sharp drop in magnitude around 10.4 μm while maintaining higher values toward 8 μm and 13 μm . This sudden decrease in absorption occurs around the absorption peak of SiO₂, which results in an abrupt change in its complex refractive index profile and therefore leaves it a challenging task to achieve very high absorptions around 10.4 μm . To partially mitigate these effects and increase the absorption throughout this range, we start by performing two parametric studies, as discussed below. Following that, in Section 3.2, we fully mitigate this challenge using the five-layer configuration.

At the dip wavelength (around 10.4 μm), the absorption level is around 30%. While this value is still quite high, we first perform a modal analysis at this wavelength to explore the possibility of increasing the absorption level by matching the momentum of such modes through surface patterning. This study provides us with initial periodicities of around 6.2 μm and 4.8 μm for TE and TM modes. Consequently, for the first parametric study, we investigate the impact of varying the periodicity of the structure while parameter “ d ” is kept unchanged at 0.3 μm . The absorption profiles are illustrated in Figure 3A for periodicities of 1.5, 2.5, 3.5,

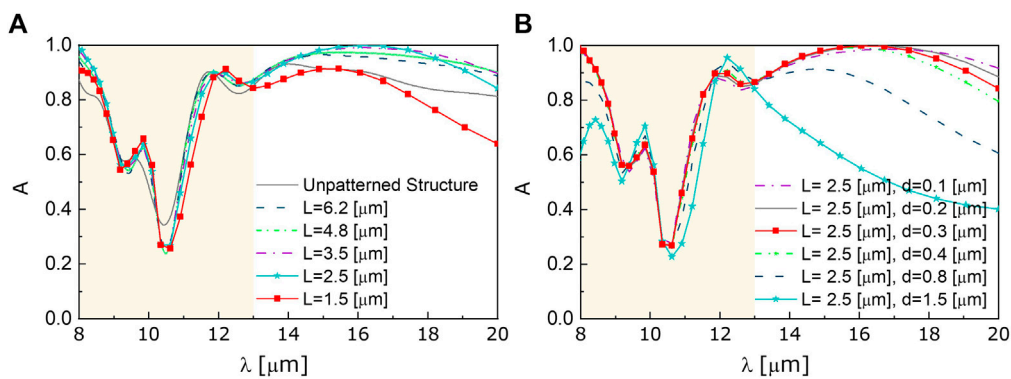


FIGURE 3 (A) Absorption spectra for the four-layer structure shown in Fig.1(A) for hot state and for (A) different periodicities and (B) for different values of “d”, as listed in the legends. In panel (A) the absorption spectrum of the unpatterned structure is also shown for comparison (gray line). The shaded area in both panels indicate the first atmospheric transparency window of 8–13 μm.

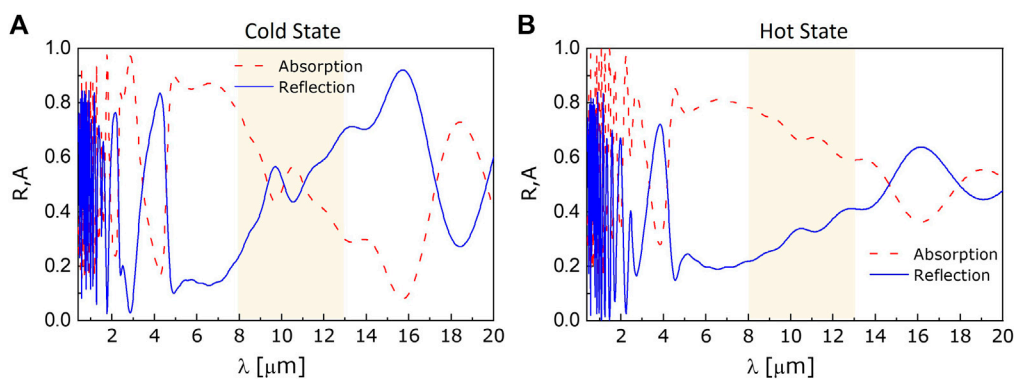


FIGURE 4 Absorption (red-dashed) and reflection (blue-solid) spectra for the five-layer structure shown in Fig.1(D) at (A) cold and (B) hot states.

4.8, and 6.2 μm. As can be seen, the examined periodicities show a similar overall behavior without a significant change in the absorption characteristics of the four-layer structure. Among these, the period of 1.5 μm seems to decrease the absorption within the higher wavelength range, which is not a desired effect. The structure with a period of 2.5 μm reaches the highest overall absorption within 8–20 μm (and simultaneously has a high reflection profile in the 0.4–2.5 μm range).

It is worth mentioning that while the periodicity of the patterned structure can (partially) fulfill the momentum matching requirement, we note that the efficiency of coupling is strongly dependent on the shape and size of the surface elements, as well as the nature of the excited modes (Abass et al., 2012). In the second parametric study, we keep the period fixed at 2.5 μm and inspect the effect of changing “d” (the distance between VO₂ patches) on the absorption spectra. The distance is changed between 0.1, 0.2, 0.3, 0.4, 0.8, and 1.5 μm, as illustrated in Figure 3B. The results indicate that as we increase “d” from 0.1 to 1.5 μm, the absorption behavior around 13 μm is almost unchanged; however, for d = 0.3 μm, almost perfect absorption is achieved at 8 μm and across

the 14–17 μm range. For larger values of “d” (0.8 and 1.5 μm), we observe a significant drop in the absorption intensities, consistent with the fact that the overall surface area of VO₂ is very small in these cases.

The study shows that even for the case of d = 0.3 μm, the sudden decrease in absorption around 10.4 μm is still present, which may not be ideal for radiative cooling purposes. To alleviate this effect and achieve a high absorption throughout the entire atmospheric transparency window (i.e., 8–13 μm), we next introduce a five-layer structure composed of a metal-insulator-metal segment, as shown in Figure 1D.

3.2 Five-layer structure

The five-layer structure consists of an additional Al₂O₃ thin film. Al₂O₃ shows an absorption peak around 17 μm (E.D. Palik et al., 1998), small absorption within the 8–13 μm range, and no significant absorption within the visible and near-infrared spectrum. As discussed in Section 2.2, the thicknesses of layers

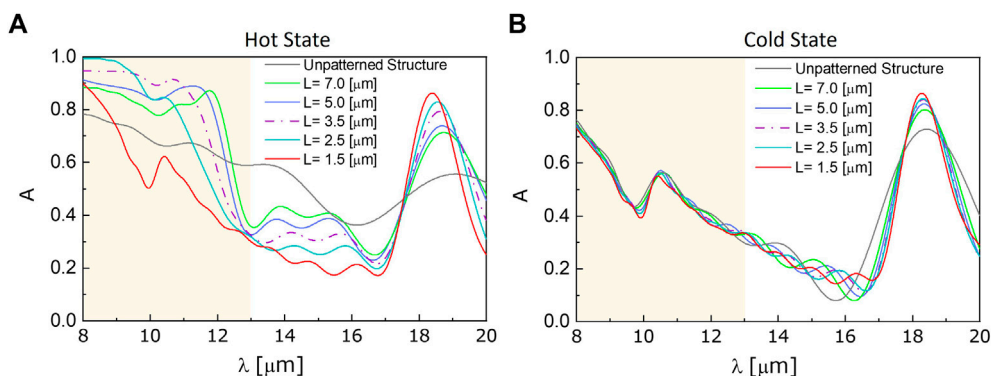


FIGURE 5 Absorption spectra for the five-layer structure shown in Figure 1E for (A) hot state and (B) cold state, for different periodicities of the VO₂ patches, as listed in the legends.

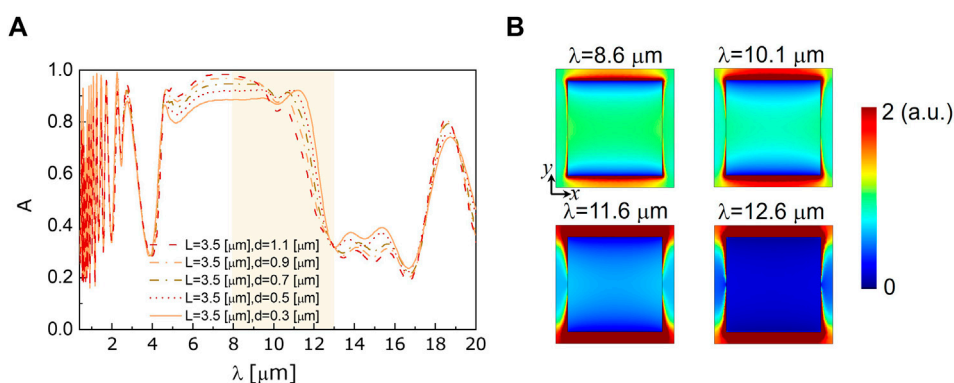


FIGURE 6 (A) Absorption profiles for the five-layer patterned structure at the hot state for different values of “d”, as listed in the legend. (B) Electric field amplitude at 8.6, 10.1, 11.6, and 12.6 μm for $L = 3.5 \mu\text{m}$ and $d = 0.7 \mu\text{m}$. The incident plane wave is y-polarized, and the fields are plotted in the middle of the VO₂ layer in the x-y plane. All fields are normalized to the amplitude of the incident plane wave.

are determined through a coarse optimization step. Figure 4 illustrates the absorption and reflection spectra of the optimized five-layer structure in the cold and hot states. The undesired dip observed in the four-layer structure is not present in the hot state absorption spectra, and simultaneously, the overall absorption is lower in the cold state. Interestingly, when the VO₂ layer is not plasmonic (i.e., cold state), some spectral signature of the SiO₂ absorption peak is present in the response. Also, in both states, the reflection is highly oscillatory at shorter wavelengths, maintaining an average of approximately 50%.

Despite the increase in the absorption profile of the optimized non-patterned five-layer structure within the atmospheric window, the absorption magnitude stays below 0.8. Like the previous case, and to enhance the absorption within this range, we introduce periodicities of 1.5, 2.5, 3.5, 5, and 7 μm to the structure (see Figure 1). We note that due to the high absorption of the layered structure, the in-plane modes are highly lossy in this case. Figure 5A depicts the calculated absorption

spectra for these periodicities in the hot state. For all cases, parameter “d” is kept constant at 0.7 μm . Inspecting Figure 5A, we observe a significant improvement in the overall absorption (and strong dependency on “L”). The structure with a period of 1.5 μm experiences a sudden drop in absorption, which is due to the smaller VO₂ surface area. The structure with a periodicity of 3.5 μm shows a fairly constant absorption magnitude of around 0.9, and absorption starts to drop slightly for higher periodicities.

To see the whole picture, it is also essential to examine the effect of the patterning of the structure on the spectral responses of the cold state. Towards that end, Figure 5B shows the absorption profiles of the five-layer structure at the cold state for different periodicities. The impact of the insulator mode of VO₂ can be clearly seen within the atmospheric window. As expected, the absorption profiles in the cold state demonstrate a clear decrease in magnitude when compared with the hot state results. This is because VO₂ depicts a dielectric response here. It is also apparent from the results shown

in Figure 5B that geometric variations and introduced periodicities have no significant impact on the reduction or enhancement of the absorption profiles in the cold state.

Given the achieved high absorption magnitude, we chose to further the work by picking the period of 3.5 μm to investigate the impact of the distance between VO₂ patches (parameter “d”) through parametric studies. Figure 6A shows the results for the sweep analysis on “d” with values of 0.3, 0.5, 0.7, 0.9, and 1.1 μm . The results reveal that the absorption spectra experience blue shift for larger values of “d” (i.e., smaller VO₂ patches), with $d = 1.1 \mu\text{m}$ reaching an almost perfect rate of 0.98 for the 6–9 μm range. The near-field distribution for $L = 3.5 \mu\text{m}$ and $d = 0.7 \mu\text{m}$ is shown in Figure 6B at four wavelengths. The field amplitudes are normalized to the amplitude of the excitation plane wave. As can be seen, the main contribution of the patterning is through scattering from the edges of the plasmonic VO₂ patches into the substrate (Abass et al., 2012), while at the same time, the large scattering can increase the impedance mismatch with free space, resulting in lower absorption. So, a trade-off is present. For instance, at the operational wavelength of 12.6 μm , despite observing large scattering at the edges (Figure 6B), the absorption is still lower than the non-patterned structure (see Figure 5A).

4 Conclusion

We investigated the performance of two nanophotonic structures for adaptive radiative cooling applications. A thin layer of non-patterned or patterned VO₂ is incorporated in each design to enable the desired thermal switching between the hot state ($T > 68^\circ\text{C}$) and cold state ($T < 68^\circ\text{C}$). The structures achieve high reflectivity within the solar spectrum (0.4–2.5 μm) and simultaneously high absorption within the atmospheric transparency window (8–13 μm) in the hot state. In addition, we show that through a two-stage design process, including an initial fast optimization of the thickness of layers, we can significantly enhance and tune the overall absorption. The phase transition of VO₂ plays a crucial role in the proposed structures, enabling enhanced absorption within the atmospheric transparency window when in the metallic phase. However, when VO₂ is in the dielectric phase, our study showed insignificant tunability within the atmospheric window. The proposed five-layer structure outperformed the four-layer structure when Al₂O₃ was added in a metal-insulator-metal arrangement to the five-layer structure. This is attributed to the adverse impact of the intrinsic absorption peak of SiO₂ in the desired wavelength range. We

envision that these findings for such planar structures could find applications in radiative cooling in electronic devices and spacecrafts, especially due to their inherent compactness as well as their passive, self-adaptive performance.

Data availability statement

The original contributions presented in the study are included in the article/supplementary material, further inquiries can be directed to the corresponding author.

Author contributions

AD-B performed the FDTD simulations and NME performed FEM simulations. AD-B wrote the first draft of the manuscript. NME supervised the project. All authors contributed to the article and approved the submitted version.

Funding

This work was supported by startup funding from Chapman University.

Conflict of interest

The author(s) NME declared that they were an editorial board member of Frontiers, at the time of submission. This had no impact on the peer review process and the final decision.

The remaining authors declare that the research was conducted in the absence of any commercial or financial relationships that could be construed as a potential conflict of interest.

Publisher’s note

All claims expressed in this article are solely those of the authors and do not necessarily represent those of their affiliated organizations, or those of the publisher, the editors and the reviewers. Any product that may be evaluated in this article, or claim that may be made by its manufacturer, is not guaranteed or endorsed by the publisher.

References

- Abass, A., Le, K. Q., Alù, A., Burgelman, M., and Maes, B. (2012). Dual-interface gratings for broadband absorption enhancement in thin-film solar cells. *Phys. Rev. B* 85 (11), 115449. doi:10.1103/PhysRevB.85.115449
- Abb, M., Wang, Y., Traviss, D., Bruck, R., de Groot, C. H., Chong, H., et al. (2014). Plasmonics and metamaterials with transparent conducting oxides. *ECS Trans.* 64 (9), 291. doi:10.1149/06409.0291ecst
- Araki, K., and Zhang, R. Z. (2022). An optimized self-adaptive thermal radiation turn-down coating with vanadium dioxide nanowire array. *Int. J. Heat Mass Transf.* 191, 122835. doi:10.1016/j.ijheatmasstransfer.2022.122835
- Assaworrorarit, S., Omair, Z., and Fan, S. (2022). Nighttime electric power generation at a density of 50 mW/m² via radiative cooling of a photovoltaic cell. *Appl. Phys. Lett.* 120 (14), 143901. doi:10.1063/5.0085205
- Bijarniya, J. P., Sarkar, J., and Maiti, P. (2020). Review on passive daytime radiative cooling: Fundamentals, recent researches, challenges and opportunities. *Renew. Sustain. Energy Rev.* 133, 110263. doi:10.1016/j.rser.2020.110263
- Butakov, N. A., Valmianski, I., Lewi, T., Urban, C., Ren, Z., Mikhailovsky, A. A., et al. (2018). Switchable plasmonic – dielectric resonators with metal – insulator transitions. *ACS Photonics* 5, 371–377. doi:10.1021/acsp Photonics.7b00334
- Cai, L., Du, K., Qu, Y., Luo, H., Pan, M., Qiu, M., et al. (2018). Nonvolatile tunable silicon-carbide-based midinfrared thermal emitter enabled by phase-changing materials. *Opt. Lett.* 43 (6), 1295–1298. doi:10.1364/ol.43.001295
- Chamoli, S. K., Li, W., Guo, C., and ElKabbash, M. (2022). Angularly selective thermal emitters for deep subfreezing daytime radiative cooling. *Nanophotonics* 11 (16), 3709–3717. doi:10.1515/nanoph-2022-0032

- Choi, M., Seo, J., Yoon, S., Nam, Y., Lee, J., and Lee, B. J. (2022). All-day radiative cooling using a grating-patterned PDMS film emitter. *Appl. Therm. Eng.* 214, 118771. doi:10.1016/j.applthermaleng.2022.118771
- Comsol (2023). Comsol. <https://www.comsol.com>
- Cui, Y., Ke, Y., Liu, C., Chen, Z., Wang, N., Zhang, L., et al. (2018). Thermochromic VO₂ for energy-efficient smart windows. *Joule* 2 (9), 1707–1746. doi:10.1016/j.joule.2018.06.018
- Currie, M., Mastro, M. A., and Wheeler, V. D. (2018). Atomic layer deposition of vanadium dioxide and a temperature-dependent optical model. *J. Vis. Exp.* 2018 (135), e57103. doi:10.3791/57103
- Didari, A., and Mengüç, M. P. (2018). A biomimicry design for nanoscale radiative cooling applications inspired by *Morpho didius* butterfly. *Sci. Rep.* 8 (1), 16891. doi:10.1038/s41598-018-35082-3
- Didari-Bader, A., and Menguc, P. (2023). "Near-field radiative transfer for biologically inspired structures," in *Light, plasmonics and particles*. Editors M. Pinar Menguc and M. Francoeur (Amsterdam, Netherlands: Elsevier). Available at: <https://www.elsevier.com/books/light-plasmonics-and-particles/menguc/978-0-323-99901-4>.
- Estakhri, N. M., and Norris, T. B. (2021). Tunable quantum two-photon interference with reconfigurable metasurfaces using phase-change materials. *Opt. Express* 29 (10), 14245–14259. doi:10.1364/oe.419892
- Fan, S., and Li, W. (2022). Photonics and thermodynamics concepts in radiative cooling. *Nat. Photonics* 16 (3), 182–190. doi:10.1038/s41566-021-00921-9
- Gentle, A., Tai, M., White, S., Arnold, M., Cortie, M. B., and Smith, G. B. (2018). Design, control, and characterisation of switchable radiative cooling. *Proc. SPIE New Concepts Sol. Therm. Radiat. Convers. Reliab.* 10759, 107590L. doi:10.1117/12.2323877
- Goldstein, E. A., Raman, A. P., and Fan, S. (2017). Sub-ambient non-evaporative fluid cooling with the sky. *Nat. Energy* 2, 17143. doi:10.1038/nenergy.2017.143
- Howes, A., Zhu, Z., Curie, D., Avila, J. R., Wheeler, V. D., Haglund, R. F., et al. (2020). Optical limiting based on Huygens' metasurfaces. *Nano Lett.* 20, 4638–4644. doi:10.1021/acs.nanolett.0c01574
- Irfan Lone, M., and Jilte, R. (2021). A review on phase change materials for different applications. *Mater. Today Proc.* 46, 10980–10986. doi:10.1016/j.matpr.2021.02.050
- Jin, Y., Jeong, Y., and Yu, K. (2022). Infrared-reflective transparent hyperbolic metamaterials for use in radiative cooling windows. *Adv. Funct. Mater.* 33, 2207940. doi:10.1002/adfm.202207940
- Kecebas, M. A., Menguc, M. P., Kosar, A., and Sendur, K. (2017). Passive radiative cooling design with broadband optical thin-film filters. *J. Quantitative Spectrosc. Radiat. Transf.* 198, 179–186. doi:10.1016/j.jqsrt.2017.03.046
- Kim, D. H., Lee, G. J., Heo, S. Y., Son, S., Kang, K. M., Lee, H., et al. (2021). Ultra-thin and near-unity selective emitter for efficient cooling. *Opt. Express* 29 (20), 31364–31375. doi:10.1364/oe.438662
- Ko, B., Badloe, T., and Rho, J. (2021). Vanadium dioxide for dynamically tunable photonics. *ChemNanoMat* 7 (7), 713–727. doi:10.1002/cnma.202100060
- Lee, K. W., Lim, W., Jeon, M. S., Jang, H., Hwang, J., Lee, C. H., et al. (2022). Visibly clear radiative cooling metamaterials for enhanced thermal management in solar cells and windows. *Adv. Funct. Mater.* 32 (1), 2105882. doi:10.1002/adfm.202105882
- Lewis, B. G., and Paine, D. C. (2000). Applications and processing of transparent conducting oxides. *MRS Bull.* 25 (8), 22–27. doi:10.1557/mrs2000.147
- Li, B., Camacho-Morales, R., Li, N., Tognazzi, A., Gandolfi, M., de Ceglia, D., et al. (2023). Fundamental limits for transmission modulation in VO₂ metasurfaces. *Photonics Res.* 11 (1), B40–B49. doi:10.1364/prj.474328
- Li, J., Wang, X., Liang, D., Xu, N., Zhu, B., Li, W., et al. (2022). A tandem radiative/evaporative cooler for weather-insensitive and high-performance daytime passive cooling. *Sci. Adv.* 8 (32), eabq0411. doi:10.1126/sciadv.abq0411
- Long, L., Taylor, S., and Wang, L. (2020). Enhanced infrared emission by thermally switching the excitation of magnetic polariton with scalable microstructured VO₂ metasurfaces. *ACS Photonics* 7 (8), 2219–2227. doi:10.1021/acsp Photonics.0c00760
- Lumerical (2023). Material database in FDTD and MODE. Available at: <https://www.lumerical.com/>.
- Matlab (2023). Matlab. Available at: <https://www.mathworks.com/products/matlab.html>
- Morin, F. J. (1959). Oxides which show a metal-to-insulator transition at the neel temperature. *Phys. Rev. Lett.* 3 (1), 34–36. doi:10.1103/PhysRevLett.3.34
- Ono, M., Chen, K., Li, W., and Fan, S. (2018). Self-adaptive radiative cooling based on phase change materials. *Opt. Express* 26 (18), A777–A787. doi:10.1364/oe.26.00a777
- Palik, E. D. (1998). *Handbook of the optical constants of solids*. San Diego, CA, USA: Academic Press, vol. I, II, and III
- Perrakis, G., Tasolamprou, A. C., Kenanakis, G., Economou, E. N., Tzortzakos, S., and Kafesaki, M. (2020). Passive radiative cooling and other photonic approaches for the temperature control of photovoltaics: A comparative study for crystalline silicon-based architectures. *Opt. Express* 28 (13), 18548–18565. doi:10.1364/oe.388208
- Qin, M., Xiong, F., Aftab, W., Shi, J., Han, H., and Zou, R. (2022). Phase-change materials reinforced intelligent paint for efficient daytime radiative cooling. *iScience* 25 (7), 104584. doi:10.1016/j.isci.2022.104584
- Raman, A. P., Anoma, M. A., Zhu, L., Rephaeli, E., and Fan, S. (2014). Passive radiative cooling below ambient air temperature under direct sunlight. *Nature* 515 (7528), 540–544. doi:10.1038/nature13883
- Sato, D., and Yamada, N. (2019). Review of photovoltaic module cooling methods and performance evaluation of the radiative cooling method. *Renew. Sustain. Energy Rev.* 104, 151–166. doi:10.1016/j.rser.2018.12.051
- Song, Y., Xu, Q., Liu, X., Xuan, Y., and Ding, Y. (2022). High-performance thermal energy storage and thermal management via starch-derived porous ceramics-based phase change devices. *Int. J. Heat Mass Transf.* 197, 123337. doi:10.1016/j.ijheatmasstransfer.2022.123337
- Sun, K., Riedel, C. A., Wang, Y., Urbani, A., Simeoni, M., Mengali, S., et al. (2018a). Metasurface optical solar reflectors using AZO transparent conducting oxides for radiative cooling of spacecraft. *ACS Photonics* 5 (2), 495–501. doi:10.1021/acsp Photonics.7b00991
- Sun, K., Riedel, C. A., Urbani, A., Simeoni, M., Mengali, S., Zalkovskij, M., et al. (2018b). VO₂ thermochromic metamaterial-based smart optical solar reflector. *ACS Photonics* 5 (6), 2280–2286. doi:10.1021/acsp Photonics.8b00119
- Sun, K., Vassos, E., Yan, X., Wheeler, C., Churm, J., Wiecha, P. R., et al. (2022a). Wafer-scale 200 mm metal oxide infrared metasurface with tailored differential emissivity response in the atmospheric windows. *Adv. Opt. Mater.* 10 (17), 2200452. doi:10.1002/adom.202200452
- Sun, K., Xiao, W., Wheeler, C., Simeoni, M., Urbani, A., Gaspari, M., et al. (2022b). VO₂ metasurface smart thermal emitter with high visual transparency for passive radiative cooling regulation in space and terrestrial applications. *Nanophotonics* 11 (17), 4101–4114. doi:10.1515/nanoph-2022-0020
- Sun, X., Sun, Y., Zhou, Z., Alam, M. A., and Bermel, P. (2017). Radiative sky cooling: Fundamental physics, materials, structures, and applications. *Nanophotonics* 6 (5), 997–1015. doi:10.1515/nanoph-2017-0020
- Tognazzi, A., Gandolfi, M., Li, B., Ambrosio, G., Franceschini, P., Camacho-Morales, R., et al. (2023). Opto-thermal dynamics of thin-film optical limiters based on the VO₂ phase transition. *Opto-thermal Dyn. thin-film Opt. limiters based VO₂ phase transition* 13 (1), 41–52. doi:10.1364/ome.472347
- Wan, C., Horak, E. H., King, J., Salman, J., Zhang, Z., Zhou, Y., et al. (2018). Limiting optical diodes enabled by the phase transition of vanadium dioxide. *ACS Photonics* 5 (7), 2688–2692. doi:10.1021/acsp Photonics.8b00313
- Wan, C., Zhang, Z., Woolf, D., Hessel, C. M., Rensberg, J., Hensley, J. M., et al. (2019). On the optical properties of thin-film vanadium dioxide from the visible to the far infrared. *Ann. Phys.* 531 (10), 1900188. doi:10.1002/andp.201900188
- Wan, C., Zhang, Z., Salman, J., King, J., Xiao, Y., Yu, Z., et al. (2021). Ultrathin broadband reflective optical limiter. *Laser and Photonics Rev.* 15 (6), 2100001. doi:10.1002/lpor.2021000011
- Wang, Q., Rogers, E. T. F., Gholipour, B., Wang, C. M., Yuan, G., Teng, J., et al. (2016). Optically reconfigurable metasurfaces and photonic devices based on phase change materials. *Nat. Photonics* 10 (1), 60–65. doi:10.1038/nphoton.2015.247
- Wang, T., Wu, Y., Shi, L., Hu, X., Chen, M., and Wu, L. (2021). A structural polymer for highly efficient all-day passive radiative cooling. *Nat. Commun.* 12 (1), 365. doi:10.1038/s41467-020-20646-7
- Xia, S.-X., Zhai, X., Huang, Y., Liu, J. Q., Wang, L. L., and Wen, S. C. (2017). Multi-band perfect plasmonic absorptions using rectangular graphene gratings. *Opt. Lett.* 42 (15), 3052–3055. doi:10.1364/ol.42.003052
- Xia, S., Zhai, X., Wang, L., Xiang, Y., and Wen, S. (2022). Plasmonically induced transparency in phase-coupled graphene nanoribbons. *Phys. Rev. B* 106 (7), 075401. doi:10.1103/PhysRevB.106.075401
- Yin, H., Yao, H., Jia, Y., Wang, J., and Fan, C. (2021). Realization of efficient radiative cooling in thermal emitter with inorganic metamaterials. *J. Phys. D Appl. Phys.* 54 (34), 345501. doi:10.1088/1361-6463/ac0659
- Zha, W., Zhu, Y., Ma, B., Yu, J., Ghosh, P., Qiu, M., et al. (2022). Nonvolatile high-contrast whole long-wave infrared emissivity switching based on In₃SbTe₂. *ACS Photonics*. doi:10.1021/acsp Photonics.2c00714
- Zhang, Y., Gurzadyan, G. G., Umair, M. M., Wang, W., Lu, R., Zhang, S., et al. (2018). Ultrafast and efficient photothermal conversion for sunlight-driven thermal-electric system. *Chem. Eng. J.* 344, 402–409. doi:10.1016/j.cej.2018.03.098
- Zhao, B., Hu, M., Ao, X., Xuan, Q., and Pei, G. (2020). Spectrally selective approaches for passive cooling of solar cells: A review. *Appl. Energy* 262, 114548. doi:10.1016/j.apenergy.2020.114548